

Nonequilibrium Singlet-Triplet Kondo Effect in Carbon Nanotubes

J. PAASKE^{1*}, A. ROSCH², P. WÖLFLE³, N. MASON^{4,5}, C. M. MARCUS⁵ AND J. NYGÅRD,¹

¹The Niels Bohr Institute & The Nano-Science Center, University of Copenhagen, DK-2100 Copenhagen, Denmark

² Institut für Theoretische Physik, Universität zu Köln, 50937 Köln, Germany

³ Institut für Theorie der Kondensierten Materie, Universität Karlsruhe, 76128 Karlsruhe, Germany

⁴ Department of Physics, University of Illinois at Urbana Champaign, Urbana IL 61801-3080, USA

⁵ Department of Physics, Harvard University, Cambridge MA 0213, USA

*e-mail: paaske@fys.ku.dk.

(Dated: April 20, 2021)

The Kondo-effect is a many-body phenomenon arising due to conduction electrons scattering off a localized spin¹. Coherent spin-flip scattering off such a quantum impurity correlates the conduction electrons and at low temperature this leads to a *zero-bias* conductance anomaly^{2,3}. This has become a common signature in bias-spectroscopy of single-electron transistors, observed in GaAs quantum dots^{4,5,6,7,8,9} as well as in various single-molecule transistors^{10,11,12,13,14,15}. While the zero-bias Kondo effect is well established it remains uncertain to what extent Kondo correlations persist in non-equilibrium situations where inelastic processes induce decoherence. Here we report on a pronounced conductance peak observed at finite bias-voltage in a carbon nanotube quantum dot in the spin singlet ground state. We explain this *finite-bias* conductance anomaly by a nonequilibrium Kondo-effect involving excitations into a spin triplet state. Excellent agreement between calculated and measured non-linear conductance is obtained, thus strongly supporting the correlated nature of this nonequilibrium resonance.

For quantum dots accommodating an odd number of electrons, a suppression of charge-fluctuations in the Coulomb blockade regime leads to a local spin-1/2 degree of freedom and, when temperature is lowered through a characteristic Kondo-temperature T_K , the Kondo-effect shows up as a zero-bias peak in the differential conductance. In a dot with an even number of electrons, the two electrons residing in the highest occupied level may either form a singlet or promote one electron to the next level to form a triplet, depending on the relative magnitude of the level splitting δ and the ferromagnetic intradot exchange energy J . For $J > \delta$, the triplet state prevails and gives rise to a zero-bias Kondo peak^{7,8}, but when $\delta > J$ the singlet state is lower in energy and no Kondo effect is expected in the linear conductance. Nevertheless, spin-flip tunneling becomes viable when the applied bias is large enough to induce transitions from singlet to triplet state. Such inter-lead exchange-tunneling may give rise to Kondo correlations and concomitant conductance peaks near $V \sim \pm\delta/e$. However, since the tunneling involves excited states with a rather limited life-time, the question remains to what extent the coherence of such inelastic spin-flips and hence the Kondo-effect is maintained?

In the context of a double-dot system, a qualitative description of a finite-bias Kondo-effect, leaving out decoherence and nonequilibrium effects, was given already in Ref.16 and

finite bias conductance peaks have already been observed in carbon nanotubes^{11,14,17} as well as in GaAs quantum dots^{8,9,18}. However, for lack of a quantitative theory for this nonequilibrium resonance no characterization of the phenomenon has yet been possible. As pointed out in Refs.19,20,21, a bias induced population of the excited state (here the triplet), may change a simple finite-bias cotunneling step into a cusp in the nonlinear conductance. Therefore, in order to quantify the strength of correlations involved in such a finite-bias conductance anomaly, a proper nonequilibrium treatment will be necessary. As we demonstrate below, the qualitative signature of Kondo-correlations is a finite bias conductance peak which is markedly sharper than the magnitude of the threshold bias.

We have examined a quantum dot based on a single-wall carbon nanotube (see Fig. 1a). Electron transport measurements of the two-terminal differential conductance were carried out in a cryostat with a base electron temperature of $T_{\text{el}} \approx 80$ mK and a magnetic field perpendicular to the nanotube axis. The low temperature characteristics of the device are seen from the density plot in Fig. 1b, showing dI/dV as a function of source-drain voltage V and gate voltage V_g . The dominant blue regions of low conductance are caused by Coulomb blockade (CB) while the sloping white and red lines are edges of the CB diamonds, where the blockade is overcome by the finite source-drain bias. Moreover, white and red horizontal ridges of high conductance around zero bias are seen. These ridges occur in an alternating manner, for every second electron added to the nanotube dot. These are the Kondo resonances induced by the finite electron spin $S = 1/2$ existing for an odd number N of electrons where an unpaired electron is localized on the tube. The zero bias resonances are absent for the other regions (with even N) where the ground state spin is $S = 0$. Over most of the measured gate-voltage range (not all shown) the diamond-plot exhibits a clear four-electron periodicity, consistent with the consecutive filling of two non-degenerate subbands, corresponding to the two different sub-lattices of the rolled up graphene sheet, within each shell¹⁷. This shell-filling scheme is illustrated in Fig. 1c.

We observe inelastic cotunneling features for all even N at $eV \sim \pm\Delta$ for a filled shell and $eV \sim \pm\delta$ for a half-filled shell. Reading off the addition, and excitation energies throughout the quartet near $V_g = -4.90$ V, shown in Fig. 1b, we can estimate the relevant energy-scales within a constant interaction model^{17,22,23}. We deduce a charging energy $E_C \approx 3.0$ meV, a level-spacing $\Delta \approx 4.6$ meV, a subband mismatch $\delta \approx 1.5$ meV, and rather weak intradot exchange, and intra-orbital Coulomb energies $J, dU < 0.05\delta$. The fact that $\delta > J$ is

consistent with a singlet ground-state for a half-filled shell, involving only the lower sub-band (orbital), together with a triplet at excitation energy $\delta - J$ and another singlet at energy δ . Notice that also the regions with N odd and doublet ground-state exhibit an inelastic resonance at an energy close to δ . We ascribe these to (possibly Kondo-enhanced) transitions exciting the valence electron from orbital 1 to orbital 2, but we shall not investigate these resonances in detail. Focusing on the half-filled shell, i.e. $N = 2$, Fig. 2a shows the measured line-shape, dI/dV vs. V , at $V_g = -4.90$ V and for T_{el} ranging from 81 mK to 687 mK. The conductance is highly asymmetric in bias-voltage and exhibits a pronounced peak near $V \sim \delta/e$ which increases markedly when lowering the temperature (cf. inset Fig. 2b).

For $N = 2$, we model the nanotube quantum dot by a two-orbital Anderson impurity occupied by two electrons coupled to the leads via four different tunneling amplitudes $t_{i\alpha}$, between orbitals $i = 1, 2$ and leads $\alpha = L, R$. In terms of the conduction electron density of states, ν_F , which we assume to be equal for the two leads, the tunneling induces a level-broadening $\Gamma_i = 2\pi\nu_F \sum_{\alpha} |t_{i\alpha}|^2$. In the Kondo-regime, $\Gamma_i \ll E_C$, charge fluctuations are strongly suppressed and the Anderson model becomes equivalent to a Kondo-model incorporating second order super-exchange (cotunneling) processes, like the one illustrated in Fig. 3a, in an effective exchange-tunneling interaction (see Supplementary Information, section 2). This effective model describes the possible transitions between the five lowest-lying two-electron states on the nanotube (see Fig. 3b). Since $J \ll \delta$, we neglect J altogether and assume that the four excited states are all degenerate with excitation-energy δ . The next excited state is a singlet entirely within orbital 2 with excitation energy 2δ (see Supplementary Information, section 2). Although this state is merely a factor of 2 higher in energy than the five lowest lying states, we shall neglect this and all higher lying states altogether. Since there are no spin-flip transitions connecting the ground-state singlet to the excited singlet at energy 2δ , we expect this omission to have a minute influence on the conductance for $V < 2\delta$.

In order to deal with the logarithmic singularities arising in low-order perturbation theory within the Kondo model, it is convenient to employ the so-called poor man's scaling method²⁴. As we have demonstrated earlier²⁵, this method can be generalized to deal also with non-degenerate spin-states, like a spin-1/2 in a magnetic field, as well as with nonequilibrium systems where the local spin degrees of freedom are out of thermal equilibrium with the conduction electrons in the leads. The present problem is complicated by the presence

of the two finite energy scales, eV and δ , causing the renormalization of the couplings to involve more than just scattering near the conduction electron Fermi-surfaces. To accommodate for this fact, one must allow for different renormalization at different energy scales, and the poor man's scaling method should therefore be generalized to produce a renormalization group (RG) flow of frequency dependent coupling functions. The details of this method have been presented in Refs. 25,26 and the specific RG-equations for this problem are presented in section 3 of the Supplementary Information.

These coupled nonlinear RG-equations do not lend themselves to analytical solution but may be solved numerically with relatively little effort. From this solution, we obtain renormalized coupling-functions with logarithmic peaks at certain frequencies determined by eV and δ (see e.g. Fig. 3c). Since resonant spin-flips take place only via the excited states at energy δ , Korringa-like spin-relaxation, via excitation of particle-hole pairs in the leads, partly degrades the coherence required for the Kondo-effect²⁷. Even at zero temperature, the couplings therefore remain weak and increase roughly as $1/\log(\sqrt{T^2 + \Gamma^2}/T_K)$, with Γ being the effective (V -dependent) spin-relaxation rate. Using the parameters $t_{\alpha i}$ from the fit in Fig. 4, we calculate the Kondo-temperature and the spin-relaxation rate and find that $T_K = 0.4$ mK and $\Gamma \approx 350$ mK (see Supplementary Information, sections 3-5). This in turn implies a small parameter $1/\ln[\delta/T_K] \approx 0.1$, which justifies our perturbative approach. Notice that the smallness of T_K corresponds roughly to a mere 50% reduction of the total hybridization to orbital 1 as an electron is added to the nanotube. This tiny T_K does not show up directly in the V -dependence of the nonlinear conductance, which is characterized instead by the excitation energy δ and the spin-relaxation rate Γ .

Having determined the renormalized coupling functions, the electrical current is finally calculated from the golden rule expression:

$$I = \frac{2\pi e}{\hbar} \int_{-\infty}^{\infty} d\omega \sum_{\substack{\sigma, \sigma' = \uparrow, \downarrow \\ \gamma, \gamma' = s, -1, 0, 1, s'}} |g_{R, \sigma'; L, \sigma}^{\gamma'; \gamma}(\omega)|^2 f(\omega - eV/2) (1 - f(\omega + \varepsilon_{\gamma'} - \varepsilon_{\gamma'} + eV/2)) n_{\gamma} - (V \rightarrow -V), \quad (1)$$

where n_{γ} are the nonequilibrium occupation numbers of the five impurity states and $g_{R, \sigma'; L, \sigma}^{\gamma'; \gamma}(\omega)$ is the renormalized exchange-tunneling amplitude for transferring a conduction electron from left to right lead and changing its spin from σ to σ' , while switching the impurity-state from γ to γ' . Figure 4 shows a comparison of this calculation to the

data, obtained by fitting the four tunneling amplitudes $t_{i\alpha}$ determining the unrenormalized exchange couplings. Notice that in practice the measured conductance at $V = 0$ and at $|V| \gg \delta$, together with the asymmetry between positive and negative bias, places strong constraints on these four amplitudes. The resulting fit is highly satisfactory, with only slight deviations at highest voltages.

To quantify the importance of Kondo-correlations, we compare also to plain nonequilibrium cotunneling. This unrenormalized second order tunneling mechanism clearly underestimates the conductance peak at positive bias, and most severely so at the lowest temperature. Qualitatively, simple nonequilibrium cotunneling gives rise to a cusp in the conductance which is roughly as wide as the magnitude of the threshold-bias itself. As evident from the data and analysis presented here, nonequilibrium Kondo-correlations instead produce a conductance anomaly which is sharper than the magnitude of the threshold,— that is a proper finite-bias peak.

Acknowledgements

This research was supported by the Center for Functional Nanostructures of the DFG (J. P., P. W.), by the European Commission through project FP6-003673 CANEL of the IST Priority (J. P.), by ARO/ARDA (DAAD19-02-1-0039), NSF-NIRT (EIA-0210736) (N. M., C. M. M.) and the Danish Technical Research Council (J. N.).

Competing financial interests

The authors declare that they have no competing financial interests.

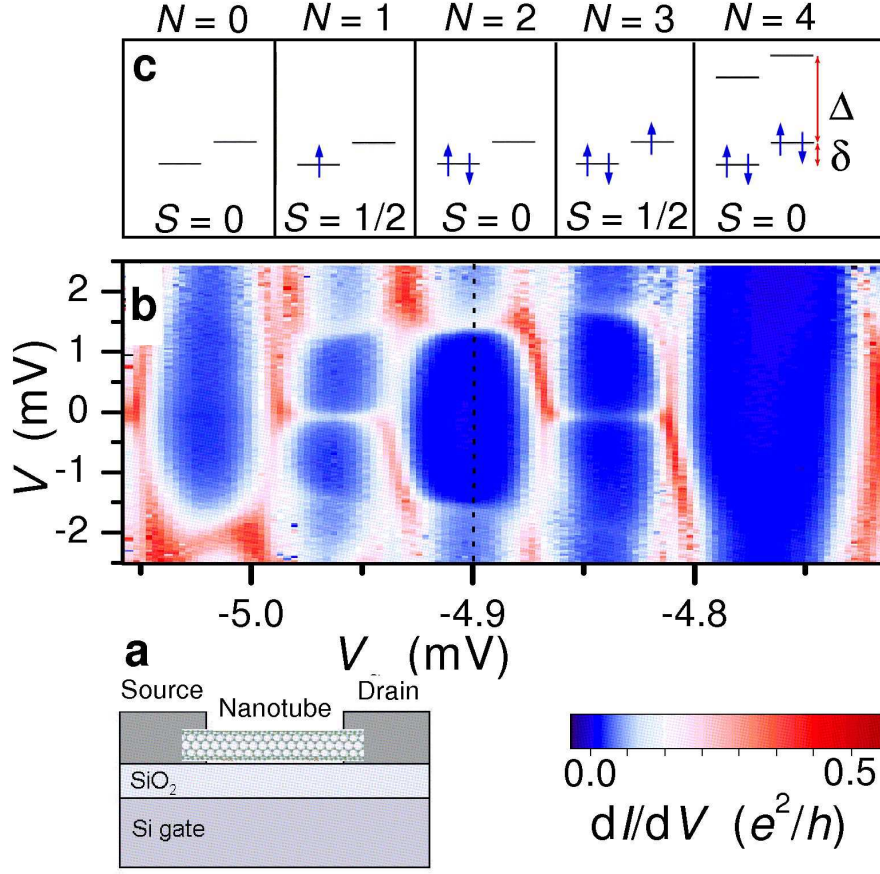


Figure 1 Experimental setup and shell-filling scheme for a single-wall carbon nanotube. **a**, Schematic of the nanotube device, comprising a single-wall carbon nanotube grown by chemical vapor deposition on a SiO₂ substrate and contacted by Cr/Au source and drain electrodes, spaced by 250 nm. Highly doped silicon below the SiO₂ cap layer acted as a back gate electrode. Room temperature measurements of conductance as a function of back-gate voltage, V_g , indicate that the conducting nanotube is metallic with a small gap outside the region considered here (cf. Supplementary Information, section 1). **b**, Density-plot of dI/dV as a function of V and V_g at $T_{el} = 81$ mK. **c**, Diagram illustrating the corresponding level-filling-scheme with N defined as the total number of electrons modulo 4.

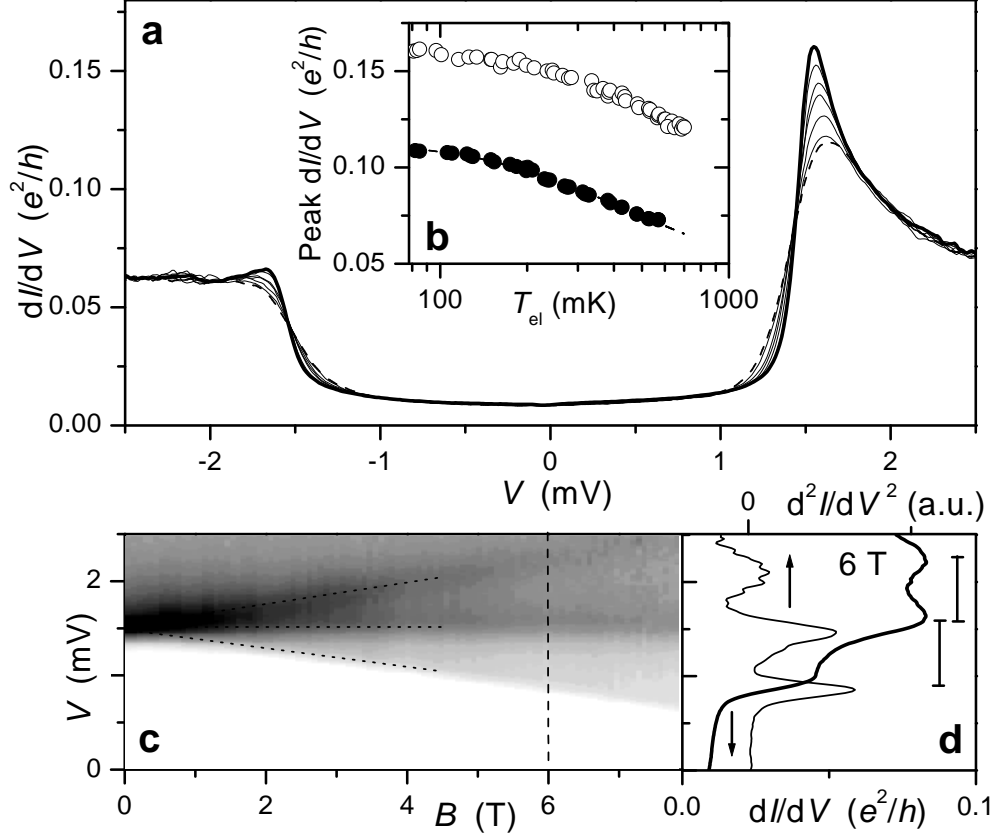


Figure 2 Temperature and magnetic field dependence of the finite-bias resonance. **a**, dI/dV as a function of V , at $V_g = -4.90$ V (dashed cross section in Fig. 1b), taken at $T_{el} = 81$ (thick), 199, 335, 388, 488, 614, 687 (dashed) mK. **b**, Temperature dependence of the finite-bias conductance peak in Fig. 2a (open circles) and the neighboring zero-bias Kondo resonance (solid circles) at $V_g = -4.96$ V (see Fig. 1a). The open circles are consistent with the saturation of a log-enhanced finite-bias Kondo-peak as T becomes smaller than the spin-relaxation rate $\Gamma \approx 350$ mK, determined from the parameters in Fig. 4. The solid circles follow the NRG-interpolation-formula $a(1 + (2^{1/0.22} - 1)(T/T_K)^2)^{-0.22}$ with $a = 0.11$ and $T_K = 1.0$ K (dashed line). **c**, dI/dV vs. V and magnetic field B , at $V_g = -4.90$ V. **d**, dI/dV vs. V at $B = 6$ T, corresponding to vertical cross section (dashed) in Fig. 2c. The d^2I/dV^2 trace (thin) underlines the presence of three distinct peaks in dI/dV . The black bars each correspond to $\Delta V = g\mu_B B/e$ with $g = 2.0$ for nanotubes.

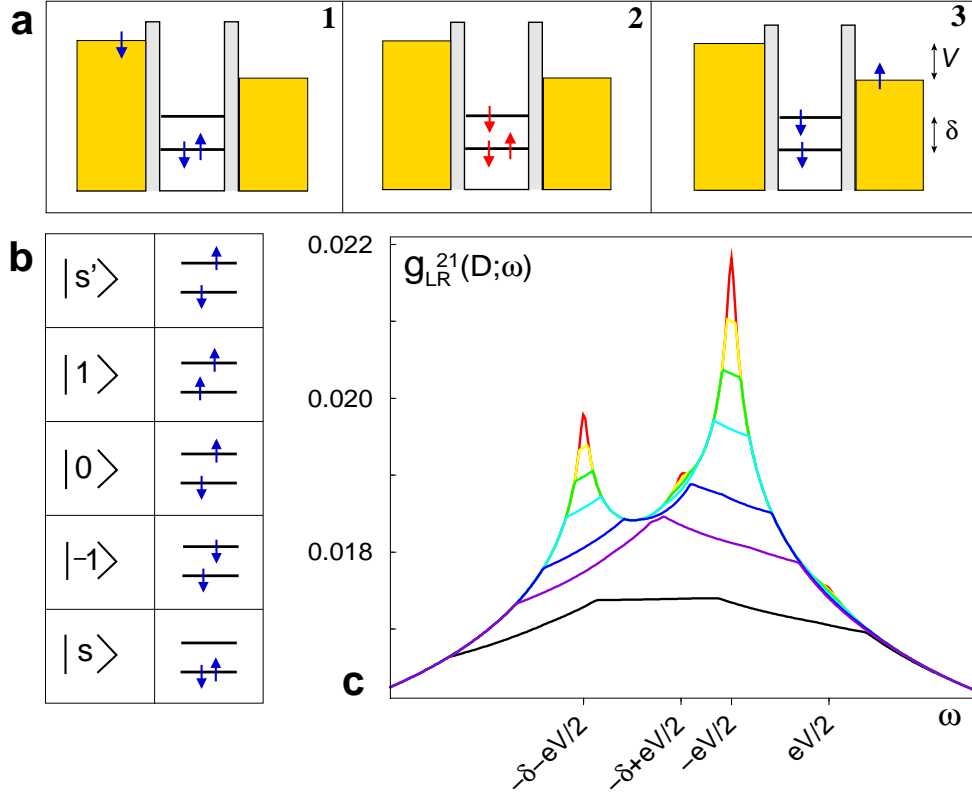


Figure 3 Schematic of the inelastic spin-exchange underlying the Kondo-effect.

a, Illustration of the cotunneling mechanism giving rise to the effective exchange-interaction in the Kondo model. Note that the virtual intermediate state (red spins) in panel 2 is suppressed by a large energy-denominator of the order of the electrostatic charging energy of the nanotube. **b**, Schematic of the five different low-energy states retained in the effective Kondo-model: $|s\rangle$ is the singlet ground-state, $|m\rangle$ ($m=1,2,3$) are the triplet components with excitation energy $\delta - J \approx \delta$ and $|s'\rangle$ is the corresponding singlet with excitation energy δ . Applying a magnetic field causes the triplet to split up as seen in Fig. 2c,d. **c**, Renormalized dimensionless exchange-coupling vs. incoming conduction electron energy ω , measuring the amplitude for exchange-tunneling from right to left lead while de-exciting an electron on the nanotube from orbital 2 to 1. Different colours encode the different stages of the RG-flow as the bandwidth is reduced from D_0 to zero. Parameters as in Fig. 4.

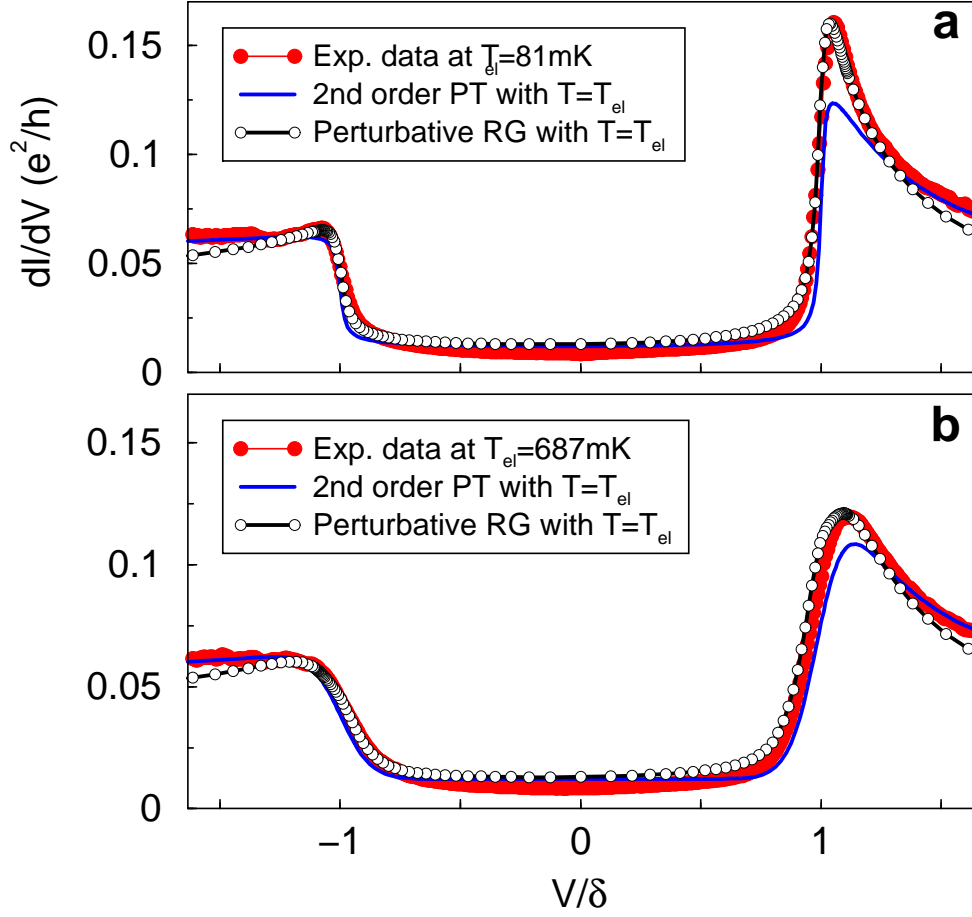


Figure 4 Fitting the nonlinear conductance by perturbative RG calculation. **a**, Experimental data (red dots) at the lowest temperature, fitted by the perturbative RG calculation (white dots) with $\{t_{L1}, t_{L2}, t_{R1}, t_{R2}\} = \{0.024, 0.033, 0.111, 0.083\}\sqrt{E_C/\nu_F}$ and $T = T_{el} = 81$ mK. We use $J = 0$ and an arbitrary bandwidth, $D_0 = 1$ eV, larger than all other energy-scales. From the bias at which dI/dV vs. V has maximum slope, we read off $\delta = 1.515$ meV. The blue curve represents simple cotunneling, i.e. second order perturbation theory (PT) with tunneling-amplitudes $t_{i\alpha}$ fitted to the data at $T = 687$ mK (see panel b). **b**, Comparing to the data (red and white dots) at the highest temperatures, using same parameters as in panel a, but with $T = T_{el} = 687$ mK. The blue curve represents the best fit of second order perturbation theory with $T = 687$ mK.

Supplementary Discussion

1. Nanotube transport experiments

Our nanotubes were grown by chemical vapor deposition (CVD) on a doped silicon substrate with a 400 nm oxide cap layer. Ferric iron nitrate nanoparticles deposited from a solution in isopropyl alcohol acted as catalyst for the CVD process, which was carried out in a tube furnace by flowing methane and hydrogen over the sample at 900 °C²⁸. This process yielded mostly individual single-wall nanotubes as determined by atomic force microscopy. The nanotubes were contacted by thermally evaporated metal electrodes (35 nm Au on 4 nm Cr), spaced by 250 nm and patterned by electron beam lithography. The two-terminal conductance was measured using standard lock-in techniques with $\sim 5 \mu\text{V}$ ac excitation and voltage bias V applied to the source with the drain grounded through a low-impedance current amplifier. The effective electron temperature can differ from the measured mixing chamber temperature in the dilution refrigerator. A base electron temperature of $T_{\text{el}} \approx 80 \text{ mK}$ was estimated from the temperature dependence of device characteristics.

In the range of gate voltage considered in this paper, the room temperature conductance of the device is around $1.8 e^2/h$ and independent of back-gate voltage V_g . At lower gate voltages, a weak V_g dependence at room temperature is seen and can be attributed to a small band gap in the metallic nanotube induced by perturbations.²⁹ The coupling decreases with V_g and at low T the Coulomb blockade peaks disappear at $V_g \sim -2.5 \text{ V}$, i.e. around $\Delta N = 40$ electrons away from the present V_g range.³⁰

2. Low energy two-particle states and effective Kondo-Hamiltonian

The relevant single-particle states of the nanotube carry spin $\sigma = \uparrow, \downarrow$ and orbital index $i = 1, 2$, and the lowest lying two-particle states are denoted as follows:

$$|s\rangle = (|\downarrow, \uparrow\rangle - |\uparrow, \downarrow\rangle) \otimes |1, 1\rangle / \sqrt{2} \quad (2)$$

$$|-1\rangle = |\downarrow, \downarrow\rangle \otimes (|1, 2\rangle - |2, 1\rangle) / \sqrt{2} \quad (3)$$

$$|0\rangle = (|\downarrow, \uparrow\rangle + |\uparrow, \downarrow\rangle) \otimes (|1, 2\rangle - |2, 1\rangle) / 2 \quad (4)$$

$$|1\rangle = |\uparrow, \uparrow\rangle \otimes (|1, 2\rangle - |2, 1\rangle) / \sqrt{2} \quad (5)$$

$$|s'\rangle = (|\downarrow, \uparrow\rangle - |\uparrow, \downarrow\rangle) \otimes (|1, 2\rangle + |2, 1\rangle) / 2 \quad (6)$$

$$|s''\rangle = (|\downarrow, \uparrow\rangle - |\uparrow, \downarrow\rangle) \otimes |2, 2\rangle / \sqrt{2} \quad (7)$$

These states have energies E_s , $E_{-1,0,1} = E_s + \delta - J$, $E_{s'} = E_s + \delta$ and $E_{s''} = E_s + 2\delta$, and since $J < \delta$, the singlet $|s\rangle$ is the ground-state. We include only the five lowest lying states and neglect the highest lying singlet, $|s''\rangle$, altogether. Within the Hilbert-space of these five states, the effective Kondo-Hamiltonian takes the form:

$$H = \sum_{\substack{\mathbf{k}, \sigma \\ i=1,2 \\ \alpha=L,R}} (\varepsilon_{\mathbf{k}} - \mu_{\alpha}) c_{\alpha i \mathbf{k} \sigma}^{\dagger} c_{\alpha i \mathbf{k} \sigma} + H_{\text{int}}$$

where

$$\begin{aligned} H_{\text{int}} = & \frac{1}{2\nu_F} \sum_{\substack{\mathbf{k}, \mathbf{k}', \sigma, \sigma' \\ i,j=1,2 \\ \alpha, \alpha'=L,R}} \{ g_{\alpha'\alpha}^{ij} \left[\delta_{ij} \vec{S} + \tau_{ij}^3 \vec{T} + \tau_{ij}^1 \vec{P}_{ij} \right] \cdot \vec{\tau}_{\sigma'\sigma} \\ & + p_{\alpha'\alpha}^{ij} \left[\delta_{ij} |s\rangle \langle s| + \frac{1}{2} (\tau_{ij}^+ |s\rangle \langle s'| + \tau_{ij}^- |s'\rangle \langle s|) \right] \delta_{\sigma'\sigma} \\ & + q_{\alpha'\alpha}^{ij} \delta_{ij} \sum_{m=-1,0,1,s'} |m\rangle \langle m| \delta_{\sigma'\sigma} \} c_{\alpha' i \mathbf{k}' \sigma'}^{\dagger} c_{\alpha j \mathbf{k} \sigma} \end{aligned} \quad (8)$$

with

$$\begin{aligned} g_{\alpha'\alpha}^{ii} &= 2\nu_F t_{i\alpha'} t_{i\alpha}^* / E_C, & g_{\alpha'\alpha}^{12} &= (g_{\alpha\alpha'}^{21})^* = 2\sqrt{2}\nu_F t_{1\alpha'} t_{2\alpha}^* / E_C, \\ p_{\alpha'\alpha}^{ii} &= \tau_{ii}^3 g_{\alpha'\alpha}^{ii}, & p_{\alpha'\alpha}^{12} &= (p_{\alpha\alpha'}^{21})^* = g_{\alpha'\alpha}^{12}, \\ q_{\alpha'\alpha}^{ij} &= 0. \end{aligned} \quad (9)$$

The vector of Pauli-matrices is denoted by $\vec{\tau}_{ij}$ and all terms in the interaction part have the form of spin, and orbital exchange, except for the two terms in the last line proportional

to $\delta_{ij}\delta_{\sigma'\sigma}$ which are pure potential scattering terms. Throughout, we use the convention $A_{\pm} = A_x \pm iA_y$, for any vector-operator \vec{A} . The Hamiltonian is expressed in terms of the two-particle vector-operators

$$\begin{aligned}
S^+ &= (S^-)^\dagger = \sqrt{2}(|1\rangle\langle 0| + |0\rangle\langle -1|), \\
S^z &= |1\rangle\langle 1| - |-1\rangle\langle -1|, \\
P_{12}^+ &= (P_{21}^-)^\dagger = \sqrt{2}|1\rangle\langle s|, \\
P_{12}^- &= (P_{21}^+)^\dagger = -\sqrt{2}|-1\rangle\langle s|, \\
P_{12}^z &= (P_{21}^z)^\dagger = -|0\rangle\langle s|, \\
T^+ &= (T^-)^\dagger = \sqrt{2}(-|1\rangle\langle s'| + |s'\rangle\langle -1|), \\
T^z &= |0\rangle\langle s'| + |s'\rangle\langle 0|,
\end{aligned}$$

together with the scalar-operators

$$\begin{aligned}
|s\rangle\langle s| &= \frac{1}{3}(P^2 - \frac{1}{2}S^2), \\
|s\rangle\langle s'| &= (|s'\rangle\langle s|)^\dagger = -\frac{1}{3}\vec{P} \cdot \vec{T}, \\
\sum_{m=-1,0,1,s'} |m\rangle\langle m| &= \frac{1}{3}(T^2 + S^2),
\end{aligned} \tag{10}$$

where $\vec{P} = \vec{P}_{12} + \vec{P}_{21}$. Defining also the operator $M = [\vec{T}, \vec{P}]/3i = i(|s\rangle\langle s'| - |s'\rangle\langle s|)$, we note that the ten operators $\{\vec{S}, \vec{T}, \vec{P}, M\}$ satisfy the commutation relations:

$$\begin{aligned}
[S_i, S_j] &= i\varepsilon_{ijk}S_k, & [S_i, T_j] &= i\varepsilon_{ijk}T_k, & [M, T_i] &= iP_i, \\
[T_i, T_j] &= i\varepsilon_{ijk}S_k, & [S_i, P_j] &= i\varepsilon_{ijk}P_k, & [M, P_i] &= -iT_i, \\
[P_i, P_j] &= i\varepsilon_{ijk}S_k, & [T_i, P_j] &= i\delta_{ij}M, & [M, S_i] &= 0.
\end{aligned} \tag{11}$$

which identifies them as generators of the Lie-algebra $SO(5)$. Notice that $T^2 + P^2 + S^2 + M^2 = 4$ is a Casimir-operator, i.e. a constant of motion. The Hamiltonian (8) is manifestly invariant under spatial rotations, but it will possess this abstract $SO(5)$ -symmetry only when $\delta = J = 0$ and $t_{1\alpha} = t_{2\alpha}$, in which case one would expect to observe a conventional zero-bias Kondo-peak, characterized by a Kondo-temperature which is enhanced compared to the usual $SU(2)$ Kondo-effect. Notice that an $SO(5)$ -Kondo-effect has been discussed earlier in the context of a triple-quantum-dot system³¹.

As pointed out for a double-dot system studied in Ref. 32, \vec{S} and \vec{P} generate $SO(4)$, and it is the addition of the excited singlet $|s'\rangle$ which adds four new generators in the

present problem. In a double-dot system at even filling, the inter-dot tunneling breaks the degeneracy between singlet and triplet states and an inelastic cotunneling channel is generally available. A finite-bias Kondo-resonance in such a double-dot system was suggested in Ref. 16 and the current due to nonequilibrium cotunneling was calculated in Ref. 21, but the combined nonequilibrium Kondo-effect has not yet been examined. By simply leaving out the excited singlet $|s'\rangle$, our present calculation could readily be applied to this problem as well.

3. Perturbative renormalization group equations

The (one-loop) perturbative renormalization group (RG) equations satisfied by the frequency dependent couplings are established in much the same way as explained earlier in Ref. 26. Here, they take the following form:

$$\frac{\partial g_{\alpha'\alpha}^{ii}(\omega)}{\partial \ln D} = - \sum_{\alpha''} \left\{ g_{\alpha'\alpha''}^{ii}(\alpha''V/2) g_{\alpha''\alpha}^{ii}(\alpha''V/2) \theta_{\omega-\alpha''V/2} + \frac{1}{2} g_{\alpha'\alpha''}^{\bar{i}\bar{i}}(\alpha''V/2) g_{\alpha''\alpha}^{\bar{i}\bar{i}}(\alpha''V/2 - \tau_{ii}^3 \delta) \theta_{\omega+\tau_{ii}^3 \delta - \alpha''V/2} \right\}, \quad (12)$$

$$\begin{aligned} \frac{\partial g_{\alpha'\alpha}^{\bar{i}\bar{i}}(\omega)}{\partial \ln D} = & - \sum_{\alpha''} \left\{ \left[g_{\alpha'\alpha''}^{ii}(\alpha''V/2) + \frac{1}{2} (p_{\alpha'\alpha''}^{ii}(\alpha''V/2) - q_{\alpha'\alpha''}^{ii}(\alpha''V/2)) \right] \right. \\ & \times g_{\alpha''\alpha}^{\bar{i}\bar{i}}(\alpha''V/2 + \tau_{ii}^3 \delta) \theta_{\omega-\tau_{ii}^3 \delta - \alpha''V/2}, \\ & + \left[g_{\alpha''\alpha}^{\bar{i}\bar{i}}(\alpha''V/2) - \frac{1}{2} (p_{\alpha''\alpha}^{\bar{i}\bar{i}}(\alpha''V/2) - q_{\alpha''\alpha}^{\bar{i}\bar{i}}(\alpha''V/2)) \right] \\ & \times g_{\alpha'\alpha''}^{\bar{i}\bar{i}}(\alpha''V/2) \theta_{\omega-\alpha''V/2} \Big\}, \end{aligned} \quad (13)$$

$$\frac{\partial p_{\alpha'\alpha}^{ii}(\omega)}{\partial \ln D} = - \frac{3}{2} \tau_{ii}^3 \sum_{\alpha''} g_{\alpha'\alpha''}^{\bar{i}\bar{i}}(\alpha''V/2) g_{\alpha''\alpha}^{\bar{i}\bar{i}}(\alpha''V/2 - \tau_{ii}^3 \delta) \theta_{\omega+\tau_{ii}^3 \delta - \alpha''V/2}, \quad (14)$$

$$\begin{aligned} \frac{\partial p_{\alpha'\alpha}^{\bar{i}\bar{i}}(\omega)}{\partial \ln D} = & - \frac{1}{2} \sum_{\alpha''} \left\{ 3 g_{\alpha'\alpha''}^{ii}(\alpha''V/2) g_{\alpha''\alpha}^{\bar{i}\bar{i}}(\alpha''V/2 + \tau_{ii}^3 \delta) \theta_{\omega-\tau_{ii}^3 \delta - \alpha''V/2} \right. \\ & + 3 g_{\alpha'\alpha''}^{\bar{i}\bar{i}}(\alpha''V/2) g_{\alpha''\alpha}^{\bar{i}\bar{i}}(\alpha''V/2) \theta_{\omega-\alpha''V/2} \\ & + \tau_{ii}^3 p_{\alpha'\alpha''}^{ii}(\alpha''V/2) p_{\alpha''\alpha}^{\bar{i}\bar{i}}(\alpha''V/2 + \tau_{ii}^3 \delta) \theta_{\omega-\tau_{ii}^3 \delta - \alpha''V/2} \\ & \left. - \tau_{ii}^3 p_{\alpha'\alpha''}^{\bar{i}\bar{i}}(\alpha''V/2) p_{\alpha''\alpha}^{\bar{i}\bar{i}}(\alpha''V/2) \theta_{\omega-\alpha''V/2} \right\}, \end{aligned} \quad (15)$$

$$\begin{aligned} \frac{\partial q_{\alpha'\alpha}^{ii}(\omega)}{\partial \ln D} = & \frac{1}{8} \tau_{ii}^3 \sum_{\alpha''} \left\{ 3 g_{\alpha'\alpha''}^{\bar{i}\bar{i}}(\alpha''V/2) g_{\alpha''\alpha}^{\bar{i}\bar{i}}(\alpha''V/2 - \tau_{ii}^3 \delta) \theta_{\omega+\tau_{ii}^3 \delta - \alpha''V/2} \right. \\ & \left. + p_{\alpha'\alpha''}^{\bar{i}\bar{i}}(\alpha''V/2) p_{\alpha''\alpha}^{\bar{i}\bar{i}}(\alpha''V/2 - \tau_{ii}^3 \delta) \theta_{\omega+\tau_{ii}^3 \delta - \alpha''V/2} \right\}, \end{aligned} \quad (16)$$

with the shorthand notation $\theta_x = \theta(D - |x|)$, $\bar{1} = 2$ and $\bar{2} = 1$. For a given set of initial

values (at scale $D = D_0$), parametrized by the bare tunneling amplitudes $t_{i\alpha}$ according to (9), these equations are readily solved numerically for arbitrary ω and D . Taking the limit of $D \rightarrow 0$, we obtain the renormalized coupling functions used in the Golden Rule expression for the current.

As usual, when deriving the Kondo-model from an Anderson model, it is convenient to introduce two angles, $(\cos \phi_i, \sin \phi_i) = (t_{iL}, t_{iR})/\sqrt{t_{iL}^2 + t_{iR}^2}$, and parameterize the exchange couplings as

$$\{g_{\alpha'\alpha}^{ij}, p_{\alpha'\alpha}^{ij}, q_{\alpha'\alpha}^{ij}\} = \{g_{ij}, p_{ij}, q_{ij}\} \begin{pmatrix} \cos \phi_i \\ \sin \phi_i \end{pmatrix} \begin{pmatrix} \cos \phi_j & \sin \phi_j \end{pmatrix}_{\alpha'\alpha} \quad (17)$$

with initial conditions $g_{ij} = 2(\nu_F/E_C)\sqrt{(1 + \tau_{ij}^1)(t_{iL}^2 + t_{iR}^2)(t_{jL}^2 + t_{jR}^2)}$, $p_{ii} = \tau_{ii}^3 g_{ii}$, $p_{12} = p_{21} = g_{12}$ and $q_{ij} = 0$. The L/R matrix-structure of the couplings is now exterior, in the sense that the RG-equations are identical for every (α', α) component.

For $D \gg \delta, V, T, \omega$, the RG-equations simplify to describe the flow of coupling constants $(g, p, q)_{ij}$ with no dependence on frequency, ω , nor lead-index, $\alpha = L, R$. The difference in tunneling-strengths to the two orbitals still plays an important role, and enters via the initial conditions. From the RG-equations it is clear that all the different couplings diverge at the same energy-scale and it is this scale which we henceforth refer to as the Kondo-temperature, T_K (see Fig. 5). The numerical solution of these high-D RG-equations allows us to study the dependence of T_K on the three independent initial values g_{11} , g_{22} and D_0 . This reveals the following nearly perfect interpolation-formula for T_K :

$$T_K \approx D_0 e^{-1/(g_{11} + g_{22} + 1.6(g_{11}^{-1} + g_{22}^{-1})^{-1})}, \quad (18)$$

where 1.6 is a good approximation to a universal number describing this particular Kondo-effect. For $g_{11} = g_{22}$ this reduces to $T_K \approx D_0 \exp(-0.36/g_{11})$, as found earlier in a study of vertical quantum dots³³(cf. also Refs. 34,35).

Notice that in the standard Kondo-effect involving a zero-bias conductance peak, the Kondo-temperature can be estimated directly from the width of the conductance peak. In the present problem, however, T_K is of little physical significance insofar as the non-linear conductance is characterized mainly by the spin-relaxation rate Γ (see sec. 5) and the subband-mismatch δ . Nevertheless, T_K still encodes a scaling-property of the RG-solutions and shows how our rather arbitrary choice of bare bandwidth $D_0 = 1$ eV is linked to

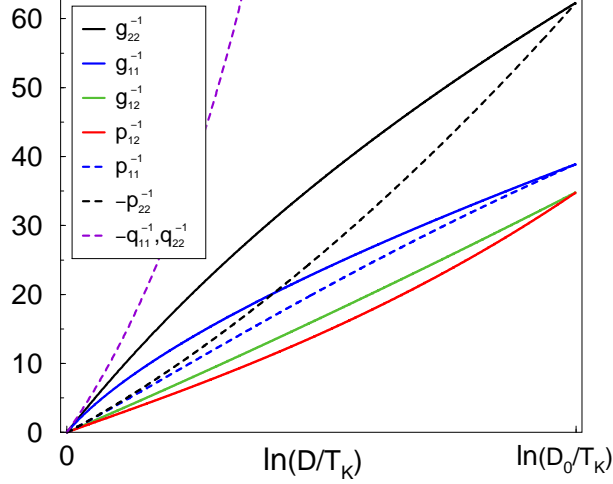


FIG. 5: **Inverse couplings vs. bandwidth D .** The inverse couplings all vanish at the same energy-scale defining T_K . The couplings shown here are based on the same bare parameters as were used for the low temperature fit in the main paper: $\{t_{L1}, t_{L2}, t_{R1}, t_{R2}\} = \{0.024, 0.033, 0.111, 0.083\}\sqrt{E_C/\nu_F}$, $J = 0$ and $D_0 = 1$ eV, which implies that $T_K \approx 0.4$ mK.

the values of the bare couplings. In spite of the fact that the Kondo-temperature in this problem is enhanced over that of the standard SU(2) symmetric Kondo-model, our fitting parameters imply that $T_K \approx 0.4$ mK, which is much smaller than the value of 1.0 K found for the neighboring Coulomb-blockade valley having an odd number of electrons on the tube (cf. Fig. 2b in main text). Estimating the effective coupling in the neighboring valley from Eq. (18) with $g_{22} = 0$, we find that this big difference in Kondo-temperature corresponds to a mere reduction of the total hybridization to orbital 1 ($\sqrt{t_{L1}^2 + t_{R1}^2}$) by roughly 50% when changing from N=1 to N=2.

4. Nonequilibrium distribution functions

Using the renormalized coupling-functions, we may calculate the transition rates between the various two-particle states using the Golden Rule expression

$$W_{\gamma'\gamma}(V, \delta, T) = \frac{2\pi}{\hbar} \int_{-\infty}^{\infty} d\omega \sum_{\substack{\sigma, \sigma'=\uparrow, \downarrow \\ \alpha, \alpha'=L, R}} |g_{\alpha'\sigma'; \alpha, \sigma}^{\gamma'; \gamma}(\omega)|^2 f(\omega - \mu_\alpha) (1 - f(\omega + \varepsilon_\gamma - \varepsilon_{\gamma'} - \mu_{\alpha'})), \quad (19)$$

where f denotes the Fermi-function. The nonequilibrium distribution functions for the two-particle states, n_γ , are then found by solving the steady-state quantum Boltzmann equation

$$\sum_{\gamma'} W_{\gamma\gamma'} n_{\gamma'} = \sum_{\gamma'} W_{\gamma'\gamma} n_{\gamma}, \quad (20)$$

together with the constraint $\sum_{\gamma=s,-1,0,1,s'} n_{\gamma} = 1$, ensuring that the two electrons in the half-filled shell on the nanotube occupy exactly one of the five lowest two-particle states. These voltage-dependent distribution functions are subsequently plugged into the Golden Rule expression for the current.

5. Spin-relaxation

As demonstrated in Ref. 27, a finite bias gives rise to Korringa-like spin-relaxation via inter-lead particle-hole excitations and for a single spin-1/2 the logarithmic singularities were found to be cut off by the (V-dependent) spin-relaxation rates $1/T_{1,2}$. To be more precise, it is the broadening of the transverse dynamical susceptibility, $1/T_2$, which cuts off the log-renormalization of spin-flip exchange couplings, whereas the renormalization of non-spin-flip exchange couplings are contained by the broadening of the longitudinal susceptibility, $1/T_1$. Diagrammatically, these rates arise from a combination of both self-energy, and vertex corrections to the spin-susceptibility bubble and a simplification which simply omits the vertex corrections will lead to serious mistakes.

In the present problem, the inter-orbital transition-rates (from excited to ground-state) are strongly enhanced by the large available phase-space. $W_{s,m}$ ($m = -1, 0, 1$) and $W_{s,s'}$ turn out to be larger than all other transition-rates by roughly an order of magnitude and the self-energy broadenings or line-widths of the excited states are therefore much larger than that of the ground-state. At least one of these large self-energy broadenings will contribute to the cut-off in the log-renormalization of all exchange couplings except one. p_{ii} couples the ground-state to itself and the relevant self-energy broadening is very weak. For this particular coupling, vertex corrections will now play the dominant role and they supply additional terms in the total broadening involving the large $W_{s,m}$ and $W_{s,s'}$. All log-singularities are therefore cut off by rates of the order of these dominant line-widths of the excited states.

From the expression for the current (cf. main text Eq.(1)), it is clear that the conductance peak at $V \sim \delta$ is mainly determined by the inter-orbital exchange-couplings $g^{\bar{ii}}$ and $p^{\bar{ii}}$. Furthermore, these couplings turn out to be larger than the others and altogether the

main influence of spin-relaxation on the physical current is therefore via these inter-orbital couplings. In other words, broadening all log-renormalization by a single effective spin-relaxation rate estimated from an inter-orbital susceptibility is expected to produce only minute errors.

In terms of a generalized ss' -susceptibility, we determine the physical spin-relaxation-rate $\Gamma_{s,s'}$ as the sum of self-energy, and vertex corrections:

$$\Gamma_{ss'} = \Gamma_v^{s,s'} + \frac{1}{2} \left(\sum_{\gamma' \neq s} W_{\gamma',s} + \sum_{\gamma' \neq s'} W_{\gamma',s'} \right), \quad (21)$$

where $\Gamma_v^{s,s'}$ is the contribution from vertex corrections. Just as the vertex-corrections to the transverse spin-susceptibility for a single spin-1/2 include only non-spin-flip processes²⁷, the correction $\Gamma_v^{s,s'}$ picks up only intra-orbital transition-rates and is therefore negligible compared to the dominant term $W_{s,s'}$ coming from the self-energy broadening of the excited state. Γ_{sm} ($m = -1, 0, 1$) is determined in a similar way and since these two different inter-orbital relaxation rates turn out to be very close in magnitude as well as in V -dependence we define a single effective spin-relaxation rate as their average:

$$\Gamma = \frac{1}{2} (\Gamma_{ss'} + \Gamma_{s0}). \quad (22)$$

The spin-relaxation mechanism is incorporated in the RG-equations by replacing θ_x by $\theta(D - |\sqrt{x^2 + T^2 + \Gamma^2}|)$ in Eqs. (12-16). Furthermore, all Fermi-functions occurring in the transition-rates and the current are effectively smeared by Γ , by replacing the energy-conserving δ -functions appearing in the Golden rule expressions with Lorentzians of width Γ (i.e. spin-susceptibilities $\text{Im}[\chi^R]$). For example, we evaluate the transition rate W_{ST} as follows:

$$\begin{aligned} W_{ST}(V, \delta, T) &= \frac{2\pi}{\hbar} \sum_{\substack{\sigma, \sigma' = \uparrow, \downarrow \\ \alpha, \alpha' = L, R}} \int_{-\infty}^{\infty} d\omega \int_{-\infty}^{\infty} d\varepsilon |g_{\alpha', \sigma'; \alpha, \sigma}^{\gamma'; \gamma}(\omega)|^2 f(\omega - \mu_\alpha) (1 - f(\omega + \varepsilon - \mu_{\alpha'})) \text{Im}[\chi_{ST}^R(\varepsilon)] \\ &\approx \frac{2\pi}{\hbar} \sum_{\substack{\sigma, \sigma' = \uparrow, \downarrow \\ \alpha, \alpha' = L, R}} \int_{-\infty}^{\infty} d\omega \int_{-\Lambda + \delta}^{\Lambda + \delta} d\varepsilon \left(\frac{1}{\mu_\alpha - \mu_{\alpha'} + \varepsilon} \int_{\mu_{\alpha'} - \varepsilon}^{\mu_\alpha} d\omega' |g_{\alpha', \sigma'; \alpha, \sigma}^{\gamma'; \gamma}(\omega')|^2 \right) \\ &\quad \times f(\omega - \mu_\alpha) (1 - f(\omega + \varepsilon - \mu_{\alpha'})) \frac{\Gamma/\pi}{(\varepsilon - \delta)^2 + \Gamma^2} \\ &\approx \frac{2\pi}{\hbar} \sum_{\substack{\sigma, \sigma' = \uparrow, \downarrow \\ \alpha, \alpha' = L, R}} \int_{\mu_{\alpha'} - \delta}^{\mu_\alpha} d\omega' |g_{\alpha', \sigma'; \alpha, \sigma}^{\gamma'; \gamma}(\omega')|^2 \int_{-\Lambda}^{\Lambda} d\varepsilon (1 + N(\varepsilon + \mu_\alpha - \mu_{\alpha'} + \delta)) \frac{\Gamma/\pi}{\varepsilon^2 + \Gamma^2}, \quad (23) \end{aligned}$$

where N is the Bose-function and $\Lambda = \sqrt{\delta^2 + J^2 + V^2 + T^2}$ is an ultra-violet cut-off on the spin-susceptibility ensuring convergence of the integral over ε . Notice that, in order to speed up the numerical evaluation, we have replaced the square of the coupling-function by its average over the window set by the Fermi-functions. The error introduced by this approximation is estimated to be subleading in the small parameter $1/\log(\delta/T_K)$.

We find that $\Gamma(V = \delta) \approx 350$ mK (varying between 345 mK and 475 mK when changing V over the measured range) and the data clearly sample the full crossover from low to high temperatures with $T_{\text{el}}^{\text{lowest}} \approx 81$ mK $< \Gamma < 687$ mK $\approx T_{\text{el}}^{\text{highest}}$.

-
- ¹ Hewson, A. C. *The Kondo Problem to Heavy Fermions*. (Cambridge University Press, 1993).
 - ² Glazman, L. & Raikh, M. Resonant Kondo transparency of a barrier with quasilocal impurity states. JETP Letters **47**, 452 (1988).
 - ³ Ng, T. & Lee, P.A. On-site coulomb repulsion and resonant tunneling. Phys. Rev. Lett. **61**, 1768 (1988).
 - ⁴ Goldhaber-Gordon, D. *et al.* Kondo effect in a single-electron transistor. Nature **391**, 156 (1998).
 - ⁵ Cronenwett, S. M., Oosterkamp, T. H. & Kouwenhoven, L. P. A tunable Kondo effect in quantum dots. Science **281**, 540 (1998).
 - ⁶ van der Wiel, W. G. *et al.* The Kondo effect in the unitary limit. Science **289**, 2105 (2000).
 - ⁷ Sasaki, S. *et al.* Kondo effect in an integer-spin quantum dot. Nature **405**, 764 (2000).
 - ⁸ Kogan, A., Granger, G., Kastner, M. A. & Goldhaber-Gordon, D. Singlettriplet transition in a single-electron transistor at zero magnetic field. Phys. Rev. B **67**, 113309 (2003).
 - ⁹ Zumbühl, D. M., Marcus, C. M., Hanson, M. P. & Gossard, A. C. Cotunneling spectroscopy in few-electron quantum dots. Phys. Rev. Lett. **93**, 256801 (2004).
 - ¹⁰ Park, J. *et al.* Coulomb blockade and the Kondo effect in single-atom transistors. Nature **417**, 722 (2002).
 - ¹¹ Nygård, J., Cobden, D. H. & Lindelof, P. E. Kondo physics in carbon nanotubes. Nature **408**, 342 (2000).
 - ¹² Liang, W., Shores, M. P., Bockrath, M., Long, J. R. & Park, H. Kondo resonance in a single-molecule transistor. Nature **417**, 725 (2002).
 - ¹³ Yu, L. H. *et al.*, Inelastic electron tunneling via molecular vibrations in single molecule transis-

- tors. Phys. Rev. Lett. **93**, 266802 (2004).
- ¹⁴ Babić, B., Kontos, T. & Schönenberger, C. Kondo effect in carbon nanotubes at half filling. Phys. Rev. B **70**, 235419 (2004).
 - ¹⁵ Jarillo-Herrero, P. *et al.* Orbital Kondo effect in carbon nanotubes. Nature **434**, 484 (2005).
 - ¹⁶ Kiselev, M. N. ,Kikoin, K. & Molenkamp, L. W. Resonance kondo tunneling through a double quantum dot at finite bias, Phys. Rev. B **68** 155323 (2003).
 - ¹⁷ Liang, W., Bockrath, M. & Park, H. Shell filling and exchange coupling in metallic single-walled carbon nanotubes. Phys. Rev. Lett. **88**, 126801 (2002).
 - ¹⁸ Jeong, H., Chang, A. M. & Melloch, M. R. The Kondo Effect in an Artificial Quantum Dot Molecule. Science **293**, 2221 (2001).
 - ¹⁹ Wegewijs, M. R. & Nazarov, Yu. V. Inelastic co-tunneling through an excited state of a quantum dot. cond-mat/0103579.
 - ²⁰ Paaske, J., Rosch, A. & Wölfle, P. Nonequilibrium transport through a Kondo dot in a magnetic field: perturbation theory. Phys. Rev. B **69**, 155330 (2004).
 - ²¹ Golovach, V. N. & Loss, D., Transport through a double quantum dot in the sequential tunneling and cotunneling regimes, Phys. Rev. B **69** 245327 (2004).
 - ²² Oreg, Y. , Byczuk, K. & Halperin, B. I. Spin configurations of a carbon nanotube in a nonuniform external potential. Phys. Rev. Lett. **85**, 365 (2000).
 - ²³ Sapmaz, S. *et al.* Electronic excitation spectrum of metallic carbon nanotubes. Phys. Rev. B **71**, 153402 (2005).
 - ²⁴ Anderson, P. W. A poor man's derivation of scaling laws for the Kondo problem. J. Phys. C **3**, 2436 (1966).
 - ²⁵ Rosch, A., Paaske, J.,Kroha, J. & Wölfle, P. Nonequilibrium transport through a Kondo dot in a magnetic field: perturbation theory and poor man's scaling. Phys. Rev. Lett. **90**, 076804 (2003).
 - ²⁶ Rosch, A., Paaske, J.,Kroha, J. & Wölfle, P. The Kondo effect in non-equilibrium quantum dots: perturbative renormalization group. J. Phys. Soc. Jpn. **74**, 118 (2005).
 - ²⁷ Paaske, J.,Rosch, A.,Kroha, J. & Wölfle, P. Nonequilibrium transport through a Kondo dot: decoherence effects. Phys. Rev. B **70**, 155301 (2004).
 - ²⁸ Hafner, J. H., Cheung, C.-L., Oosterkamp, T. H. & Lieber, C. M. High-yield assembly of individual single-walled carbon nanotube tips for scanning probe microscopies. J. Phys. Chem.

- B **105**, 743 (2001).
- ²⁹ Minot, E. D., Yaish, Y., Sazonova, V. & McEuen, P. L. Determination of electron orbital magnetic moments in carbon nanotubes. *Nature* **428**, 536 (2004).
 - ³⁰ Jarillo-Herrero, P. *et al.* Electronic Transport Spectroscopy of Carbon Nanotubes in a Magnetic Field. *Phys. Rev. Lett.* **94**, 156802 (2005).
 - ³¹ Kuzmenko, T., Kikoin, K. & Avishai, Y. Dynamical Symmetries in Kondo Tunneling through Complex Quantum Dots, *Phys. Rev. Lett.* **89**, 156602 (2002).
 - ³² Kikoin, K. & Avishai, Y. Kondo tunneling through real and artificial molecules. *Phys. Rev. Lett.* **86**, 2090 (2001).
 - ³³ Pustilnik, M., & Glazman, L. I., Conduction through a quantum dot near a singlet-triplet transition. *Phys. Rev. Lett.* **85** 2993 (2000).
 - ³⁴ Eto, M. & Nazarov, Y. V., Multiparameter scaling of the Kondo effect in quantum dots with an even number of electrons, *Phys. Rev. B* **66** 153319 (2002).
 - ³⁵ Golovach, V. N. & Loss, D., Kondo effect and singlet-triplet splitting in coupled quantum dots in a magnetic field, *Europhys. Lett.* **62** 83 (2003).